Controlling light emission by a thermalized ensemble of colloidal quantum dots with a metasurface

Hector Monin, Aurelian Loirette–Pelous, Eva de Leo, Aurelio A Rossinelli, Ferry Prins, David J Norris, Elise Bailly, Jean-Paul Hugonin, Benjamin Vest, Jean-Jacques Greffet

To be published in Optics Express:

Title:	Controlling light emission by a thermalized ensemble of colloidal quantum dots with a metasurface
Authors:	Hector Monin,Aurelian Loirette--Pelous,Eva De Leo,Aurelio Rossinelli,Ferry Prins,David Norris,Elise Bailly,Jean-Paul Hugonin,benjamin vest,Jean-Jacques Greffet
Accepted:	09 December 22
Posted	15 December 22
DOI:	https://doi.org/10.1364/OE.471744

Controlling light emission by a thermalized ensemble of colloidal quantum dots with a metasurface

HECTOR MONIN,[1] AURELIAN LOIRETTE-PELOUS,[1] EVA DE LEO,[2] AURELIO A. ROSSINELLI,[2] FERRY PRINS,[2] DAVID J. NORRIS, [2] ELISE BAILLY, [1] JEAN-PAUL HUGONIN,[1] BENJAMIN VEST,[1] AND JEAN-JACQUES GREFFET,[1,*]

[1] *Université Paris-Saclay, Institut d'Optique Graduate School, CNRS, Laboratoire Charles Fabry, 91127, Palaiseau, France*

[2] *Optical Materials Engineering Laboratory, Department of Mechanical and Process Engineering, ETH Zurich, 8092 Zurich, Switzerland*

[*] *jean-jacques.greffet@institutoptique.fr*

Abstract: We report an experimental and theoretical study of light emission by a patterned ensemble of colloidal quantum dots (cQDs). This system modifies drastically the emission spectrum and polarization as compared to a planar layer of cQDs. It exhibits bright, directional and polarized emission including a degree of circular polarization in some directions. We introduce a model of light emission based on a local Kirchhoff law which reproduces accurately all the features of the experiment. The model provides a figure of merit to assess quantitatively the emitted power. This work paves the way to the systematic design of efficient ultrathin light emitting metasurfaces with controlled polarization, spectrum and directivity.

1. Introduction

The control of light emission from single emitters via resonators is a widespread topic in the scientific literature of the past 70 years. Theoretical concepts and tools have been developed as early as the 1940's, with Purcell's seminal paper on the modification of spontaneous emission probability at radio frequencies [1]. The process of cavity mediated emission has since then been extended to the visible domain of the electromagnetic spectrum [2]. Within the field of cavity quantum electrodynamics, milestones are the enhancement of spontaneous emission [3], its inhibition [4–6], the observation of the strong coupling regime through the signature of mode splitting [7] and the Rabi oscillation regime [8]. The concepts explored by cavity QED have been generalized in the community of nanophotonics with emitters interacting with other types of "cavities" such as antennas [9–11] or photonic crystals [12, 13], that can similarly tailor the electromagnetic environment to affect the properties of light emission. Among the properties that can be engineered through emitter-resonator interaction, one notes the spontaneous rate of emission [14–17], the directivity of emission [18–21], or the emission spectrum [22–26].

Demonstration of higher power and control of directivity at the single emitter level as well as the technical feasability and reproducibility of fabrication processes naturally paves the way towards the design of light-emitting metasurfaces consisting of a large number of emitters embedded in a metasurface. Metasurfaces are based on planar arrays of antennas, whose modes are engineered to provide control over the spatial, spectral and polarization response. A survey of important contributions can be found in ref. [27] for light emission by fluorophores in metasurfaces and in ref. [28] for light extraction from semiconductors.

The purpose of this paper is to consider a particular case of metasurface consisting of an ensemble of colloidal quantum dots structured into a resonant dielectric grating. The system of

quantum dots is thus both an ensemble of incoherent quantum dots emitting light by spontaneous emission and a resonant dielectric grating. We analyse how this system shapes the spectrum, the directivity and the polarization of the emitted light.

When designing or analysing the interplay between single emitters and metasurfaces, the standard approach outlined in ref. [27] is to consider that each emitter can be treated as a dipolar emitter. Its environment is thus taken into account to analyse its emission, via, for instance, the Purcell effect.

In our study, we are dealing with a metasurface, behaving as an extended resonator, and fabricated using an ensemble of closely packed QDs. If the emitters have a broad emission spectrum, an environment with narrower resonances may modify significantly the emission spectrum [29]. This modification is position-dependent in a resonant metasurface. One could thus first imagine to model the light emitted from the ensemble of emitters as an average of the emission pattern of single emitters over position and dipole moment orientation. Nevertheless, this approach leads to particularly lengthy calculations and misses a crucial point: in such a system, the emitters are both sources but are also the very material that the resonator consists of, shaping the environment that the emitters radiate into. The optical properties of the quantum dot layer must be accurately accounted for. Additionally, the absolute amplitude of light emitted by cQDs remains unknown when treated as single dipolar emitters: the "single emitter" approach does not provide an upper bound of the emitted power.

The generalized Kirchhoff's law approach enables to overcome the previous limitations [30]. It is based on the description of the emission by first calculating the absorption features of the structure. Under this formalism, ensemble of emitters are described not as randomly positioned and randomly oriented dipoles, but as forming a layer with optical properties affecting the mode structure of the system. Since the model is based on the local absorptivity within the structure, an upper bound for absorption (and therefore for emission) can be assessed by maximizing the absorptivity.

All in all, the generalized Kirchhoff's law approach is able to adequately model the interplay between a metasurface and an *ensemble* of emitters, and explains all the resonance effects and features observed experimentally, as will be shown in the main part of this paper. In this article, we use this model to discuss our observations and analyze the data. We present the experimental data in the next section. The third section is devoted to the introduction of the model, and we compare data with theory in the fourth section.

2. Experiments

System description

We study in this paper the emission of light by the system depicted in Fig. 1. The major feature of the structure is its top 1D quantum-dot grating (QDG). This grating was fabricated using a template-stripping technique. In a first step, a dispersion of CdSe based cQDs was drop-casted onto a silicon template in which the negative shape of the grating was etched away [31, 32]. After evaporation of the solvent, a SiO_2 glass slide was attached with epoxy adhesive to the back of the QDG. In a final step, the whole stack was removed from the silicon template using mechanical cleavage.

The cQDs used in the experiment were synthesized in the laboratory, following procedures and methods reported in previous works of the authors [31]. They consist of a CdSe core, inside a CdS/ZnS shell (2 monolayers + 2 monolayers), for a total diameter of around 10 nm. This sets the absorption peak maximum around 620 nm.

The whole structure is therefore made of a dense ensemble of cQDs whose solvent has evaporated. It consists of the grating itself, with alternating lines and grooves with a groove depth of 50 nm and a duty cycle of 50%. The period of the structure is denoted as a, and its value taken as 400 nm or 450 nm depending on the sample under study. The grating lies atop a

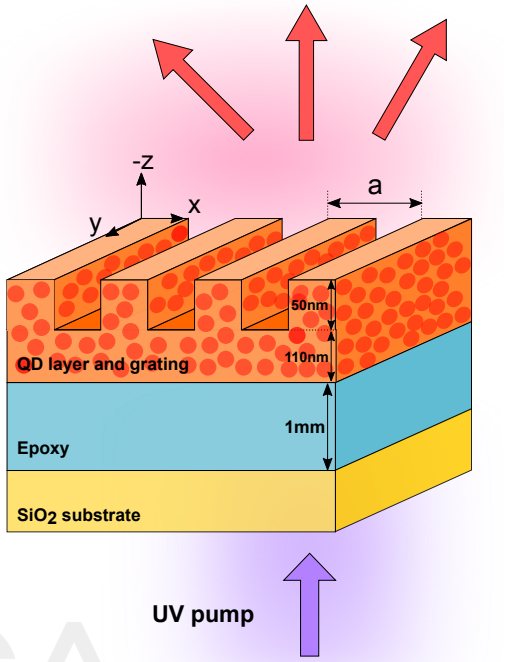

Fig. 1. **Schematic view of the QDG system.** The whole QDG is patterned on a SiO_2 substrate. The top layer, comprising both the grating and the supporting slab, is made of the very same closely packed quantum dots, left as a dense ensemble of emitters after evaporation of the solvent. The system is pumped by a UV LED illuminating the structure from the backside, via the substrate.

110 nm thick uniform layer of colloidal quantum dots (cQDs) with an absorption peak around 620 nm. Details regarding the cQDs and the fabrication process of the QDG are also available in the Supplemental Document.

The photoluminescence (PL) properties, and in particular, the spatial and spectral features of the light emission by such a system have been characterized experimentally using the setup depicted in Fig. 2. The cQD layer was optically excited by a UV LED illuminating the back of the sample. A microscope objective focuses the beam through the substrate and epoxy onto the cQD layer. The PL is then collected and collimated by another microscope objective facing the grating.

In this study, we are interested in getting information on three characteristics of light emission: spectrum, directivity, and polarization. All the information we are looking for is accessible by performing Fourier imaging and using a spectrometer.

2.1. PL intensity map

In a first set of experiments, we focus on spectral and angular features. We use appropriate optics to image the Fourier plane of the collection objective onto the input slit of a spectrometer. This slit selects a narrow area of the Fourier plane that corresponds to a wide range of emission directions in the grating direction, that is the x axis. Dispersion by the spectrometer grating forms an image on the CCD camera sensor that corresponds to a PL map of the system with respect to both wavelength and direction of emission.

Results are depicted on Fig. 3a, showing the total PL intensity as a function of wavelength

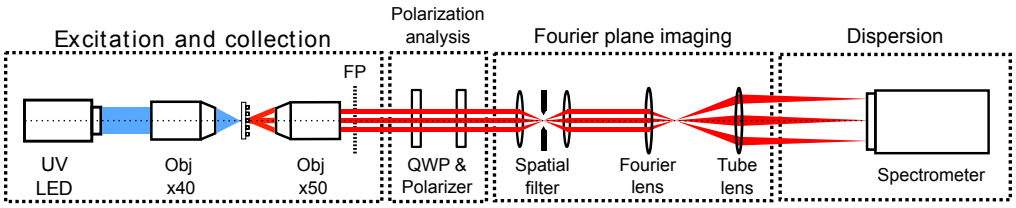

Fig. 2. **Schematic depiction of the experimental setup.** The setup uses a microscope to illuminate the back of the sample with UV light. The light is collected by a microscope objective with large numerical aperture (NA=0.8). The whole apparatus allows switching between direct imaging and back focal plane (hereafter called Fourier plane) imaging by the insertion of a Fourier lens. The Fourier plane can also be imaged on the input slit of a spectrometer. In this configuration, the image formed on the spectrometer detector is a wavevector versus wavelength plot of the PL collected from the excited sample.

and emission angle $\sin(\theta) = ck_x/\omega$, for a sample of period a=400 nm. Different features can be observed on this map. The most prominent feature is arguably a bright cross-shaped pattern, formed by the intersection of two branches. A second cross, fainter and blue-shifted, is also visible. The brightest spot of the main cross is located at the close to the crossing point, indicating that the maximum of emitted intensity occurs at a direction normal to the surface of the QDG, for a wavelength around 648 nm. More generally, the bright cross feature can be interpreted in terms of narrowband and directional emission by plotting vertical cross sections of the map. When one considers emission away from the crossing point, emission takes place mainly in two lobes, symmetric with respect to the normal direction.

The whole pattern is superimposed on a faint isotropic emission background ranging from 610 nm to 670 nm. This emission has its maximum at 640 nm, and is consistent with the PL emission spectrum from a bare layer of cQDs. This is shifted from the position of the absorption maximum of a bare layer of cQD, located at around 620 nm (see Supplemental Document). Directional emission along the cross branches is experimentally observed up to a wavelength of 690 nm where the background emission is below the noise level.

At 645nm, around 8% of the total emission within the objective's NA comes from the dispersion branches and represent funneled in the directional mode. This value goes up to 15% when looking at 660 nm, away from the center of the pattern, where the background emission has decreased more significantly than the emission in the cross branches. Thus, the contrast between the directional emission and the isotropic background tends to increase, thanks to this slight difference in spectral evolution of the two patterns. The luminance of the cross is 7 to 8 times larger than the luminance of the background at 645 nm, while this factor reaches 10 to 11 at 660 nm. Additionally, one can note that the percentage of emission coming from the directional mode would be much higher if a lower NA objective is chosen, as it would result in a significant filtering of the background emission.

Fourier imaging

Fourier imaging allows for a representation of directivity and polarization features of the spectrally integrated emission. Fig. 3b depicts intensity in the Fourier plane. The picture shows that most of the intensity is emitted along two arcs with a peak at normal incidence. An analysis of the polarization features in the Fourier plane is performed using waveplates and polarizers to measure the Stokes parameters (S_0, S_1, S_2, S_3) of the emitted light. S_0 is the total intensity. The measurement of S_0 normalized by it maximum value is displayed in Fig. 3b. S_1/S_0 is displayed on Fig 3c, and is obtained by subtracting the two intensity maps measured when placing a

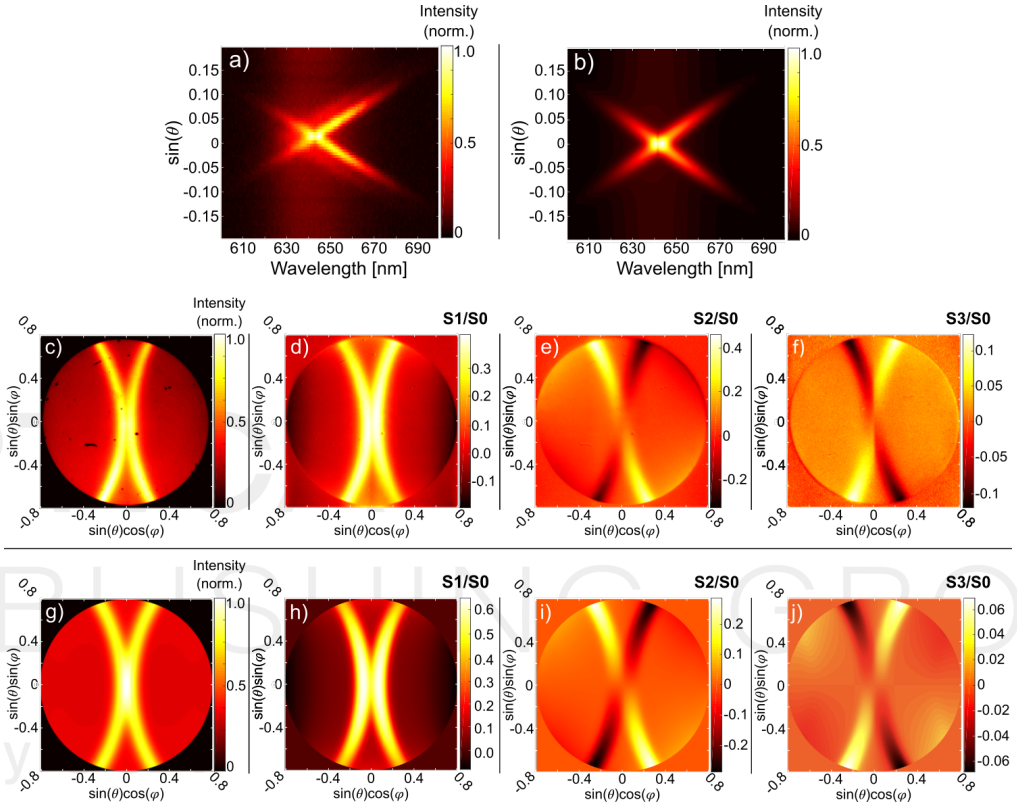

Fig. 3. **Intensity, directivity and polarization characteristics of the QDG system PL for a period a=400 nm,**. **a)** PL intensity plotted as a function of wavelength (horizontal axis) and emission direction (vertical axis), as experimentally measured. **b)** Numerical simulations of the PL intensity following the generalized Kirchhoff's modelling procedure. **c)-f)** Stokes vector components S_0, S_1/S_0, S_2/S_0, and S_3/S_0 of the emitted light, plotted as colormaps in the Fourier plane. These components fully represent the polarization state of the light emitted in all directions by the QDG system. The different maps are obtained by measuring the intensity distribution in the Fourier plane for different orientations of the quarter wave plate and polarizers, used for polarization analysis (see the experimental setup of Fig. 2). **g)-j)** Numerical simulations of the Stokes vector components, following the generalized Kirchhoff's modelling procedure.

polarizer with its axis either parallel or perpendicular to the grating grooves. Similarly, S_2/S_0 is obtained when placing the polarizer at +45° and −45° with respect to the grooves orientation (see Fig. 3d). Finally, The degree of circular polarization S_3/S_0 is shown in Fig. 3e. The parameter S_3 is obtained by subtracting the two intensity maps measured with a right and a left circular polarizers formed by combining a polarizer and a quarter wave plate.

The observation of a degree of circular polarization may be surprising as its generation is usually due to chiral samples. However, optical activity has been reported with non-chiral metasurfaces illuminated in oblique incidence [33]. The behaviour observed in our work has the same properties that in ref. [33]: dichroism is not seen at normal incidence; it changes sign in opposite directions; it takes place close to a mode resonance.

The experimental observations show unambiguously that the structure under study is able to drastically modify light emission, causing enhanced and directional outcoupling of the emission and changes in the emission spectrum. Finally, light emission is strongly polarized and may even be circularly polarized in some emission directions. In the next section, we discuss qualitatively the physical process responsible for these effects.

Qualitative interpretation of the PL features

In this section, we show that the features of the PL can be interpreted using the mode structure of the system. In our experiment, the cQDs form a slab with an effective refractive index much larger than 1 so that guided modes are supported by the slab. The cQDs are pumped by the UV light coming from the bottom of the structure so that they also behave as light emitters. The emitters can relax by spontaneous emission: they can excite either the slab modes or the radiative modes. In summary, the cQDs have two roles: on one hand, they form a corrugated planar waveguide which supports leaky modes; on the other hand, they behave as fluorophores embedded in the waveguide.

Without corrugation, light emission is only due to radiative modes. It is spatially incoherent, and provides an isotropic, unpolarized background. In the presence of a periodic corrugation, the slab modes are leaky modes so that light coupled to the slab mode is then emitted in a well-defined direction. Thus, despite the fact that all emitters are incoherent, the system generates spatially coherent (directional) emission. The origin of the spatial coherence of the field along the surface is the propagation of the leaky mode. The spatial coherence length is thus dictated by the decay length of the leaky mode [34, 35].

According to this mechanism, the emission should have the polarization of the leaky mode. This can be easily checked by analysing the polarization of the light emitted in a plane perpendicular to the grooves edges. We select light propagating in this plane by using the spectrometer slit to collect components in the $k_y = 0$ direction of the Fourier plane (defining the Oxz plane of incidence) and disperse them with the grating. The Fig. 4a provides PL maps measured as function of $\sin(\theta)$, corresponding to momentum k_x in the plane $k_y = 0$, and as a function of the wavelength. When placing a polarizer along the y direction, along the grooves, we select the TE polarization. When placing the polarizer along the x direction, we select the TM polarizarion. This was also confirmed by adding a half-wave plate after the linear polarizer. This rotates together with the linear polarizer to ensure a constant polarization orientation of the light reaching the spectrograph to remove any polarization dependence of the spectrometer's components. It can be observed non-ambiguously that the bright cross shape is associated to emission in the TE polarization, while the isotropic background remains unpolarized. A faint secondary cross can be observed in the orthogonal polarization.

We now discuss the emission pattern observed in Fig. 3b. Given the rotational symmetry of a plane, the dispersion relation of a guided mode at a given frequency has the form $k_{\mathrm{gm}} = n_{\mathrm{eff}}\omega/c$ where n_{eff} is the effective refractive index. The corresponding dispersion relation in the plane (k_x, k_y) is a circle whose radius is larger than ω/c so that it is not coupled to the far-field. This

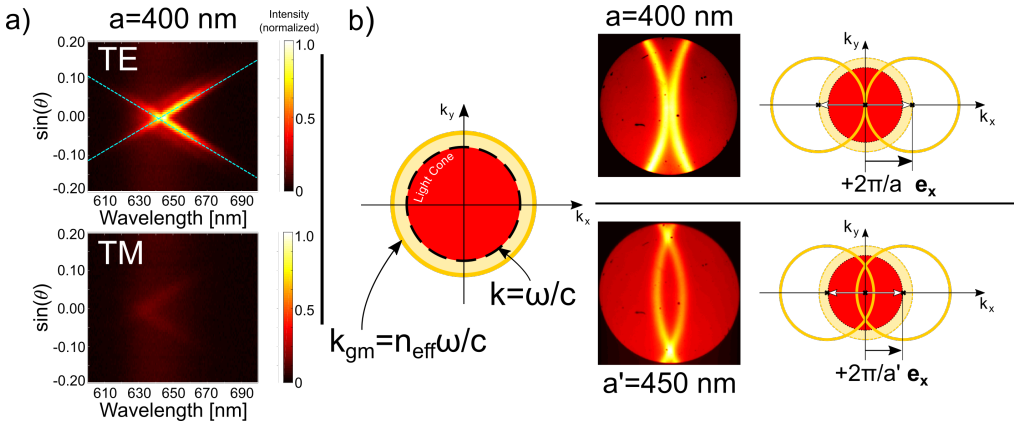

Fig. 4. **Qualitative interpretation of the experimental features in relation to the modal structure of the sample. a)** PL maps of the QDG structure for TE (top) and TM (bottom) polarization for a=400 nm. Dashed lines are plots of the dispersion relation of the guided mode for TE polarization, displaced by the grating into the light cone. **b)** Schematic description of the Fourier plane light distribution. When considered individually, the guided-mode propagation constant lies beyond the limit of the light line. The top lamellar grating couples the guided mode to modes $\mathbf{k} = \mathbf{k}_{\mathrm{gm}} \pm \frac{2\pi}{a}\mathbf{e}_x$ corresponding to circles translated by $\pm\frac{2\pi}{a}\mathbf{e}_x$. The result is displayed for two different grating periods, 400 nm and 450 nm.

is where the grating comes into play: the guided mode dispersion relation is folded back into the light cone according to $\mathbf{k} = \mathbf{k}_{\mathrm{gm}} \pm \frac{2\pi}{a}\mathbf{e}_x$ so that the dispersion relation is now given by two circles centered at $\pm\frac{2\pi}{a}\mathbf{e}_x$ as sketched in Fig. 4b. The branches of the circle that are inside the light cone become leaky and can be measured as shown in Fig. 4b for two different grating periods.

3. Light emission by a thermalized ensemble of quantum dots

The modelling of light emission by the system must include two key ingredients:

1. the emission spectrum by a homogeneous thermalized slab of emitters and
2. the emission through a resonator whose geometry and optical properties are influenced by the emitters themselves.

As discussed in ref. [27], the first step can be accounted for by using the emission spectrum of the fluorophore and the second step by computing light emission by a dipole placed in a given environment. We note that the refractive index of the environment may change under pumping so that both effects cannot be included independently under strong pumping.

A self-consistent model for light emission under pumping has been widely used for semiconductors. It is based on Kirchhoff's law [36, 37]. The emitted power is given as the product of the absorptivity by the semiconductor and the blackbody radiance. The pumping intensity is accounted for by including what is known as the photon chemical potential μ in the Bose-Einstein distribution [37] and by using the refractive index in the presence of pumping to compute the absorptivity. In the case of an LED, μ is given by the difference of the quasi-Fermi levels in the conduction band and valence band which is equal to eV where e is the electron charge and V is the applied voltage. The absorptivity depends on the occupation of the electronic states given by the Fermi-Dirac distribution of the two bands. The Kirchhoff model has enabled the design of very efficient silicon light-emitting diodes [38].

In the case of an LED, all emitting points have an equivalent environment. This is not the case for a metasurface which may have several localized resonances at different points and different frequencies. Hence, a local form of the Kirchhoff law is needed. It has been introduced in ref. [30] where a local absorption rate $\alpha(\mathbf{r})$ was introduced. The method has been applied to analyse the photoluminescence and electroluminescence of a layer of PbS cQDs on a periodic array of gold patches [39]. The Kirchhoff method assumes that the emitting system is thermalized. A discussion of the thermalisation of an ensemble of PbS cQDs as a function of the ligand size has been reported recently [40]. In the rest of the paper, we use this approach to model light emission by the QDG system. According to ref. [30], the power radiated in a specific direction θ, at a wavelength λ and in a given polarization i = TE or i = TM can be cast in the form:

$$P_e(\lambda,\theta,i,\mu) = \iiint_V \alpha_{abs}(\lambda,\theta,i,\vec{r},\mu)\, dV \frac{2hc^2}{\lambda^5} \frac{1}{\exp(\frac{hc}{k_B T\lambda} - \frac{\mu}{k_B T}) - 1}. \quad (1)$$

where k_B is Boltzmann constant, T is the temperature and $\alpha_{abs}(\lambda,\theta,i,\vec{r},\mu)$ is a local rate of absorption. Let us emphasize that the absorption involved here is the absorption of the material under UV excitation so that the populations are out of equilibrium. This term contains the entire information on the mode geometry of the system. The second term of the expression describes the emission spectrum of the cQD layer considered as an ensemble of thermalized emitters. For $\frac{hc}{\lambda} >> \mu$, we can replace the Bose-Einstein distribution by its Wien approximation:

$$P_e(\lambda,\theta,i,\mu) = \iiint_V \alpha_{abs}(\lambda,\theta,i,\vec{r},\mu)\, dV \frac{2hc^2}{\lambda^5} \exp(-\frac{hc}{k_B T\lambda}) \exp(\frac{\mu}{k_B T}). \quad (2)$$

Thus, the calculation of the emitted power can be performed by numerically computing *absorption* of incoming light within the cQD layer, instead of calculating the power *radiated* by ensembles of radiating dipoles placed in the cQD slab. To proceed, we need to know the refractive index of the material under pumping. We emphasize that computing light emission from the knowledge of the absorption spectrum requires a great accuracy of the imaginary part of the refractive index due to the exponentially varying term $\exp(-\frac{hc}{k_B T\lambda})$. A method to measure the permittivity of TDBC J-aggregated molecules (5,5',6,6'-tetrachloro-1,1'-diethyl-3,3'- di(4-sulfobutyl)-benzimidazolo-carbo cyanine) in order to reproduce photoluminescence measurements has been reported recently [41]. In this work, we used the emission data to identify the permittivity of the effective medium made of the assembly of cQDs.

4. Numerical modelling and results

The field distribution in the cQD slab, and the subsequent local absorption, depends on the geometry of the whole structure. We study the structure in the spectral range [600 nm, 700 nm]. We detail in the Supplemental document the procedure used to model the refractive indices of the different layers. We consider a duty cycle f = 50% for the top QDG in contact with air. The absorptivity is computed using a rigorous coupled-wave approximation (RCWA) method [42]. The method gives the reflected and transmitted field amplitudes for TE and TM incident plane waves of arbitrary angle and frequency. The absorption is then derived from energy conservation.

The results of the numerical simulations of the PL, normalized by the maximum intensity, are plotted in Fig. 3g. The numerical simulations of the Stokes vector components normalized by S_0 are shown in panels Fig. 3h to Fig. 3j. To allow a direct comparison between the simulations (that represent light emitted by the system) and experimental measurements (that represent light collected by the detector at the end of the experimental setup), some experimental parameters were taken into account: the instrumental response and point spread function was included in our model, as well as an unbalance between responses in TE and TM polarizations.

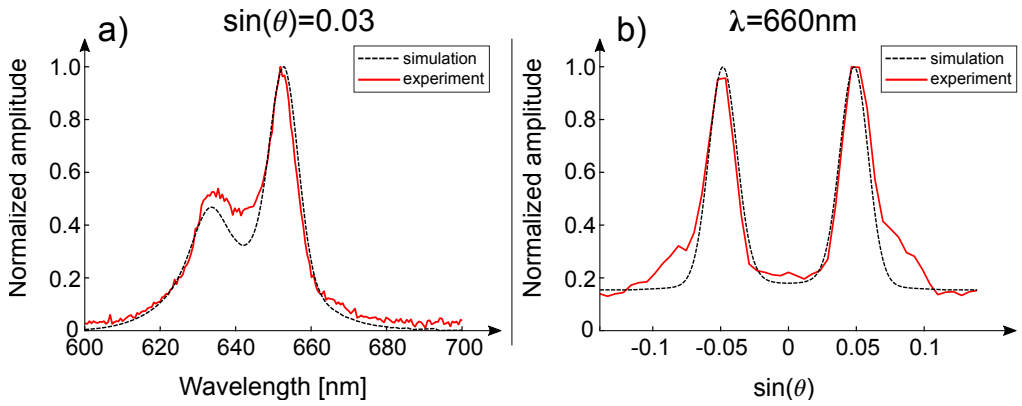

Fig. 5. **PL map cross-sections and comparison between experimental data and results obtained with the thermalized emitters model**. **a)** Spectral profile of light emitted at $\sin\theta = 0.03$. **b)** Emission diagram at $\lambda = 660\,\text{nm}$. All plots are normalized to their respective maximum intensity.

Furthermore, to show quantitatively the differences between experimental measurements and numerical simulations, we plot different cross sections (experimentally measured from Fig. 3 and numerically simulated from Fig. 3f) selecting a specific emission direction (Fig. 5a, with $\sin\theta = 0.03$) or a specific wavelength (Fig. 5b, with $\lambda = 660\,\text{nm}$).

The numerical results reproduce all major features observed on the plot: directional and spectrally narrow emission over a faint isotropic background, as well as all the polarization characteristics. Small deviations are noticeable in the relative heights of emission peaks from Fig. 5a. Those deviations are likely to be connected to experimental artifacts such as uncorrected spectral response and impulse response of the whole instrumentation chain, as well as residual deviations in the refractive index model. One can also note broader emission lobes on Fig. 5b. The lobes are formed by the contribution of the faint remaining cross pattern in the TM polarization (see Fig 4a), which is slightly offset with the bright cross pattern of the TE configuration.

5. Conclusion

In this paper, we studied the light emitted by an ensemble of quantum dots arranged in a periodically corrugated slab which can support leaky modes. When the system was pumped in the UV range, strongly polarized, spectrally narrow and directional light emission was observed. A local form of Kirchhoff's law has been used to model the system photoluminescence. This approach involves the calculation of the absorptivity of the structure. It is well suited for the design of light sources with specified properties involving dense assemblies of thermalized emitters. We note that such a model is able to account for both the electromagnetic properties of the whole resonator architecture surrounding the emitter, and for modification of the electromagnetic properties of the emitter itself, through modifications of its imaginary permittivity induced by pumping. Therefore, this model can also accurately predict light emission by systems experiencing progressively induced transparency of the emitter layer that are observed when increasing the pump power.

Funding. This work was supported by the French Agence Nationale pour la Recherche Grant No. ANR-17-CE24-0046. J.-J.G. acknowledges the support of Institut Universitaire de France. E.D.L , A.A.R., F.P., and D.J.N. were supported by the Swiss National Science Foundation under an Ambizione program grant PZ00P2-161243 and under grant no. 200021-165559.

Author contributions. JJG and EDL conceived the project. HM, ALP and EB performed modelling simulations. EDL performed samples design, fabrication, and characterization with input from FP and DN.

AR assisted in samples preparation. JJG and BV supervised the project. HM and BV wrote the original draft of the manuscript. All authors contributed to the discussion of the results and to the revision of the paper.

Disclosures. The authors declare no conflicts of interest.

Data availability. Data underlying the results presented in this paper are not publicly available at this time but may be obtained from the authors upon reasonable request.

Supplemental document. See Supplement 1 for supporting content regarding materials and methods.

References

1. E. M. Purcell, "Spontaneous Emission Probabilities at Radio Frequencies," Phys. Rev. **69**, 681 (1946).
2. K. H. Drexhage, "IV Interaction of Light with Monomolecular Dye Layers," in *Progress in Optics,* (1974), pp. 163–232.
3. P. Goy, J. M. Raimond, M. Gross, and S. Haroche, "Observation of Cavity-Enhanced Single-Atom Spontaneous Emission," Phys. Rev. Lett. **50**, 1903–1906 (1983).
4. D. Kleppner, "Inhibited spontaneous emission," Phys. Rev. Lett. **47**, 233 (1981).
5. R. G. Hulet, E. S. Hilfer, and D. Kleppner, "Inhibited spontaneous emission by a rydberg atom," Phys. Rev. Lett. **55**, 2137–2140 (1985).
6. W. Jhe, A. Anderson, E. A. Hinds, D. Meschede, L. Moi, and S. Haroche, "Suppression of Spontaneous Decay at Optical Frequencies: Test of Vacuum-Field Anisotropy in Confined Space," Phys. Rev. Lett. **58**, 1497–1497 (1987).
7. R. J. Thompson, G. Rempe, and H. J. Kimble, "Observation of normal-mode splitting for an atom in an optical cavity," Phys. Rev. Lett. **68**, 1132–1135 (1992).
8. Y. Kaluzny, P. Goy, M. Gross, J. M. Raimond, and S. Haroche, "Observation of Self-Induced Rabi Oscillations in Two-Level Atoms Excited Inside a Resonant Cavity: The Ringing Regime of Superradiance," Phys. Rev. Lett. **51**, 1175–1178 (1983).
9. P. Mühlschlegel, H.-J. Eisler, O. J. F. Martin, B. Hecht, and D. W. Pohl, "Resonant optical antennas." Sci. (New York, N.Y.) **308**, 1607–1609 (2005).
10. R. X. Bian, R. C. Dunn, X. S. Xie, and P. T. Leung, "Single Molecule Emission Characteristics in Near-Field Microscopy," Phys. Rev. Lett. **75**, 4772–4775 (1995).
11. M. S. Eggleston, K. Messer, L. Zhang, E. Yablonovitch, and M. C. Wu, "Optical antenna enhanced spontaneous emission," Proc. National Acad. Sci. **112**, 1704–1709 (2015).
12. P. Lodahl, A. Floris van Driel, I. S. Nikolaev, A. Irman, K. Overgaag, D. Vanmaekelbergh, and W. L. Vos, "Controlling the dynamics of spontaneous emission from quantum dots by photonic crystals," Nature **430**, 654–657 (2004).
13. S. Noda, M. Fujita, and T. Asano, "Spontaneous-emission control by photonic crystals and nanocavities," Nat. Photonics **1**, 449–458 (2007).
14. P. Anger, P. Bharadwaj, and L. Novotny, "Enhancement and Quenching of Single-Molecule Fluorescence," Phys. Rev. Lett. **96**, 113002 (2006).
15. S. Kühn, U. Håkanson, L. Rogobete, and V. Sandoghdar, "Enhancement of Single-Molecule Fluorescence Using a Gold Nanoparticle as an Optical Nanoantenna," Phys. Rev. Lett. **97**, 017402 (2006).
16. V. Flauraud, R. Regmi, P. M. Winkler, D. T. Alexander, H. Rigneault, N. F. Van Hulst, M. F. García-Parajo, J. Wenger, and J. Brugger, "In-plane plasmonic antenna arrays with surface nanogaps for giant fluorescence enhancement," Nano Lett. **17**, 1703–1710 (2017).
17. E. J. R. Vesseur, F. J. G. de Abajo, and A. Polman, "Broadband purcell enhancement in plasmonic ring cavities," Phys. Rev. B **82**, 165419 (2010).
18. H. Aouani, O. Mahboub, E. Devaux, H. Rigneault, T. W. Ebbesen, and J. Wenger, "Plasmonic Antennas for Directional Sorting of Fluorescence Emission," Nano Lett. **11**, 2400–2406 (2011).
19. A. G. Curto, G. Volpe, T. H. Taminiau, M. P. Kreuzer, R. Quidant, and N. F. van Hulst, "Unidirectional Emission of a Quantum Dot Coupled to a Nanoantenna," Science **329**, 930–933 (2010).
20. T. Kosako, Y. Kadoya, and H. F. Hofmann, "Directional control of light by a nano-optical Yagi–Uda antenna," Nat. Photonics **4**, 312–315 (2010).
21. E. Le Moal, S. Marguet, B. Rogez, S. Mukherjee, P. Dos Santos, E. Boer-Duchemin, G. Comtet, and G. Dujardin, "An Electrically Excited Nanoscale Light Source with Active Angular Control of the Emitted Light," Nano Lett. **13**, 4198–4205 (2013).
22. G. Vecchi, V. Giannini, and J. Gómez Rivas, "Shaping the Fluorescent Emission by Lattice Resonances in Plasmonic Crystals of Nanoantennas," Phys. Rev. Lett. **102**, 146807 (2009).
23. A. Vaskin, J. Bohn, K. E. Chong, T. Bucher, M. Zilk, D.-Y. Choi, D. N. Neshev, Y. S. Kivshar, T. Pertsch, and I. Staude, "Directional and Spectral Shaping of Light Emission with Mie-Resonant Silicon Nanoantenna Arrays," ACS Photonics **5**, 1359–1364 (2018).
24. M. Ringler, A. Schwemer, M. Wunderlich, A. Nichtl, K. Kürzinger, T. A. Klar, and J. Feldmann, "Shaping Emission Spectra of Fluorescent Molecules with Single Plasmonic Nanoresonators," Phys. Rev. Lett. **100**, 203002 (2008).
25. H. Yokoyama, K. Nishi, T. Anan, H. Yamada, S. Brorson, and E. Ippen, "Enhanced spontaneous emission from gaas quantum wells in monolithic microcavities," Appl. Phys. Lett. **57**, 2814–2816 (1990).

26. M. Suzuki, H. Yokoyama, S. D. Brorson, and E. P. Ippen, "Observation of spontaneous emission lifetime change of dye-containing langmuir–blodgett films in optical microcavities," Appl. Phys. Lett. **58**, 998–1000 (1991).
27. A. Vaskin, R. Kolkowski, A. F. Koenderink, and I. Staude, "Light-emitting metasurfaces," Nanophotonics **8**, 1151–1198 (2019).
28. G. Lozano, S. R. Rodriguez, M. A. Verschuuren, and J. Gómez Rivas, "Metallic nanostructures for efficient led lighting," Light. Sci. Appl. **5**, e16080 (2016).
29. M. Ringler, A. Schwemer, M. Wunderlich, A. Nichtl, K. Kürzinger, T. A. Klar, and J. Feldmann, "Shaping emission spectra of fluorescent molecules with single plasmonic nanoresonators," Phys. Rev. Lett. **100**, 203002 (2008).
30. J.-J. Greffet, P. Bouchon, G. Brucoli, and F. Marquier, "Light emission by nonequilibrium bodies: local kirchhoff law," Phys. Rev. X **8**, 021008 (2018).
31. F. Prins, D. K. Kim, J. Cui, E. De Leo, L. L. Spiegel, K. M. McPeak, and D. J. Norris, "Direct patterning of colloidal quantum-dot thin films for enhanced and spectrally selective out-coupling of emission," Nano Lett. **17**, 1319–1325 (2017). PMID: 28120610.
32. E. De Leo, A. A. Rossinelli, P. Marques-Gallego, L. V. Poulikakos, D. J. Norris, and F. Prins, "Polarization-based colour tuning of mixed colloidal quantum-dot thin films using direct patterning," Nanoscale **14**, 4929–4934 (2022).
33. E. Plum, X.-X. Liu, V. A. Fedotov, Y. Chen, D. P. Tsai, and N. I. Zheludev, "Metamaterials: Optical activity without chirality," Phys. Rev. Lett. **102**, 113902 (2009).
34. R. Carminati and J.-J. Greffet, "Near-field effects in spatial coherence of thermal sources," Phys. Rev. Lett. **82**, 1660–1663 (1999).
35. E. Bailly, J.-P. Hugonin, B. Vest, and J.-J. Greffet, "Spatial coherence of light emitted by thermalized ensembles of emitters coupled to surface waves," Phys. Rev. Res. **3**, L032040 (2021).
36. L. Ferraioli, P. Maddalena, E. Massera, A. Parretta, M. A. Green, A. Wang, and J. Zhao, "Evidence for generalized kirchhoff's law from angle-resolved electroluminescence of high efficiency silicon solar cells," Appl. Phys. Lett. **85**, 2484–2486 (2004).
37. P. Würfel, "The chemical potential of radiation," J. Phys.C: Solid State Phys. **15**, 3967–3985 (1982).
38. M. A. Green, J. Zhao, A. Wang, P. Reece, and M. Gal, "Efficient silicon light-emitting diodes," Nature **412**, 805–808 (2001).
39. H. Wang, A. Aassime, X. Le Roux, N. J. Schilder, J.-J. Greffet, and A. Degiron, "Revisiting the role of metallic antennas to control light emission by lead salt nanocrystal assemblies," Phys. Rev. Appl. **10**, 034042 (2018).
40. A. Caillas, S. Suffit, P. Filloux, E. Lhuillier, and A. Degiron, "Identification of two regimes of carrier thermalization in pbs nanocrystal assemblies," The J. Phys. Chem. Lett. **12**, 5123–5131 (2021). PMID: 34029086.
41. E. Bailly, K. Chevrier, C. P. de la Vega, J.-P. Hugonin, Y. D. Wilde, V. Krachmalnicoff, B. Vest, and J.-J. Greffet, "Method to measure the refractive index for photoluminescence modelling," Opt. Mater. Express **12**, 2772–2781 (2022).
42. J.-P. Hugonin and P. Lalanne, "Light-in-complex-nanostructures/reticolo: V9," (2021).